**Research Article**

# Mixed-conducting ceramic–carbonate membranes exhibiting high CO₂/O₂ permeation flux and stability at high temperatures

R. ORTEGA-LUGO[a], J. A. FABIÁN-ANGUIANO[a], O. OVALLE-ENCINIA[b],
C. GÓMEZ-YÁÑEZ[a], B. H. ZEIFERT[a], J. ORTIZ-LANDEROS[a,*]

[a]*Instituto Politécnico Nacional, Escuela Superior de Ingeniería Química e Industrias Extractivas, Departamento de Ingeniería en Metalurgia y Materiales, UPALM-Zacatenco, IPN Avenue, Mexico City 07738, Mexico*
[b]*Chemical Engineering School for Engineering of Matter, Transport and Energy, Arizona State University, Tempe, AZ 85287-6106, USA*

**Abstract:** This investigation demonstrates the feasibility to fabricate high quality ceramic–carbonate membranes based on mixed-conducting ceramics. Specifically, it is reported the simultaneous $CO_2/O_2$ permeation and stability properties of membranes constituted by a combination of ceramic and carbonate phases, wherein the microstructure of the ceramic part is composed, in turn, of a mixture of fluorite and perovskite phases. These ceramics showed ionic and electronic conduction, and at the operation temperature, the carbonate phase of the membranes is in liquid state, which allows the transport of $CO_3^{2-}$ and $O^{2-}$ species via different mechanisms. To fabricate the membranes, the ceramic powders were uniaxially pressed in a disk shape. Then, an incipient sintering treatment was carried out in such a way that a highly porous ceramic was obtained. Afterwards, the piece is densified by the infiltration of molten carbonate. Characterization of the membranes was accomplished by SEM, XRD, and gas permeation techniques among others. Thermal and chemical stability under an atmosphere rich in $CO_2$ was evaluated. $CO_2/O_2$ permeation and long-term stability measurements were conducted between 850 and 940 ℃.

The best permeation–separation performance of membranes of about 1 mm thickness, showed a maximum permeance flux of about $4.46 \times 10^{-7}$ mol·m⁻²·s⁻¹·Pa⁻¹ for $CO_2$ and $2.18 \times 10^{-7}$ mol·m⁻²·s⁻¹·Pa⁻¹ for $O_2$ at 940 ℃. Membranes exhibited separation factor values of 150–991 and 49–511 for $CO_2/N_2$ and $O_2/N_2$ respectively in the studied temperature range. Despite long-term stability test showed certain microstructural changes in the membranes, no significant detriment on the permeation properties was observed along 100 h of continuous operation.

**Keywords:** $CO_2$ separation; $O_2$ separation; ceramic–carbonate membrane; selectivity

## 1 Introduction

Greenhouse gas (GHG) emission produced by anthropogenic activities comprises the principal contribution to the global warming and its related environmental issues. Combustion of fossil fuels in thermal power plants and other chemical and manufacture industries, such as cement and steel making, are examples of big fixed sources of atmospheric $CO_2$ emissions [1–3].

* Corresponding author.
E-mail: jortizla@ipn.mx, jolanderos@gmail.com

The use of alternative sources of energy that do not involve the emission of $CO_2$ is a promising way to reduce these pollutant emissions and therefore, to contribute to sustainability. However, considering the magnitude of the so-called fossil fuel economy, the transition towards a primary use of renewable energy alternatives is certainly ambitious and could be envisaged only in the long term. Meanwhile, the development of affordable techniques, involving capture and subsequent transformation of $CO_2$ into useful chemicals, could be an important mitigation strategy.

The state of the art poses promising $CO_2$ capture techniques applied during pre-combustion and post–combustion stages (for example inorganic membrane systems), that seem to be affordable [3–5]. For instance, Sherman *et al.* [6] proposed, at a conceptual level, a combustion-assisted $CO_2$ capture process, by using a metal–carbonate dual phase membrane, to separate $CO_2$ coming from a power plant flue gas. The design of this process involves the catalytic combustion of syngas on the permeate side of the membrane. The design considers a detailed flow sheet, along with the corresponding mass and energy balances and estimated energy costs. Authors used, as a point of reference, the perm-selective performance of a membrane constituted by stainless steel–carbonate dual phase (previously described by Chang *et al.* [7]), where they reported a permeation flux of $2.5 \times 10^{-8}$ mol·s$^{-1}$·m$^{-2}$·Pa$^{-1}$ at 650 ℃. Authors concluded that, due to the energy cost associated with the operation, the membrane requires substantial improvements in the permeation flux density and stability, under useful operational conditions.

Metal–carbonate membranes can be considered as mixed electron and carbonate-ion conductor (MECC), which are able to simultaneously permeate $CO_2$ and $O_2$ through the following reversible electrochemical reaction (Eq. (1)):

$$CO_2 + \frac{1}{2}O_2 + 2e' \leftrightarrow CO_3^{2-} \qquad (1)$$
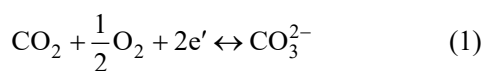
Certainly, at the feed side it is considered oxidizing stream containing carbon dioxide and oxygen, wherein at the permeate side the reverse reaction takes place to deliver a gas mixture containing a molar ratio of $CO_2 : O_2$ of $2 : 1$. Silver-based MECC has been also reported as a promising option to fabricate $CO_2$ separation membranes [8–13]. Silver–carbonate ($Li_2$–$Na_2CO_3$) system has exhibited very high $CO_2/O_2$ flux densities from 0.67/0.37 to 1.02/0.75 at 600 and 675 ℃

respectively. Manufactured by the electrochemical dealloying method, such a system presented a silver matrix with interconnected porosity [11,12]. Certain stability issues relating to the wettability features of the silver with molten carbonates can be solved by performing surface coating strategies [10,13]. Moreover, silver-based MECC membranes has been proposed as an alternative to produce syngas through a combined dry-oxy reforming catalytic reactor concept which takes advantage of the simultaneous transport of $CO_2$ and $O_2$ through the membrane [13].

Despite there are still some potential drawbacks associated with these kinds of separation technology towards its industrial application, the current studies suggest the feasibility of the use of dual-phase membranes to accomplish the goals of $CO_2$ emissions mitigation without compromise on costs [6,14]. In this sense, ceramic–carbonate membranes have showed similar performance than the metal–carbonate version and in some cases, they present better thermal and chemical stability, which can be translating into longer membrane lifetime in service [6].

Recent investigations report the high capacity of dual phase ceramic–carbonate membranes to separate $CO_2$ at intermediate and high temperatures [15–22]. Depending on the ceramic material, it serves as pure ionic or mixed ionic–electronic conductor support of an ionic conductive molten carbonate phase. Therefore, in the latter case, these membranes can be considered as a mixed ionic–electronic and carbonate-ion conductor (MIECC), which are able to simultaneously permeate $CO_2$ and $O_2$ by three different mechanisms. $CO_2$ permeation results from the reaction between the oxygen ions coming from the ceramic oxide (ionic conduction properties) with the $CO_2$ molecules in the feed gas; as this involves the production of carbonate ions (Eq. (2)), these species are transported through the molten carbonates driven by a chemical gradient. Subsequently, in the downstream side of the membrane, the reversible takes place, which involves the release of $CO_2$ as the permeate gas and the recombination of oxygen ion species with vacancies in the bulk ceramic.

$$CO_2 + O_O^x \leftrightarrow CO_3^{2-} + V_{\ddot{O}} \qquad (2)$$
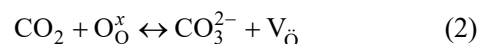
On the other hand, like the case of metal-based MECC membranes, with both $O_2$ and $CO_2$ in the feed, the simultaneous permeation of $CO_2$ and $O_2$ takes place following reversible electrochemical reaction (Eq. (1)) but in this case taking advantage of the electronic
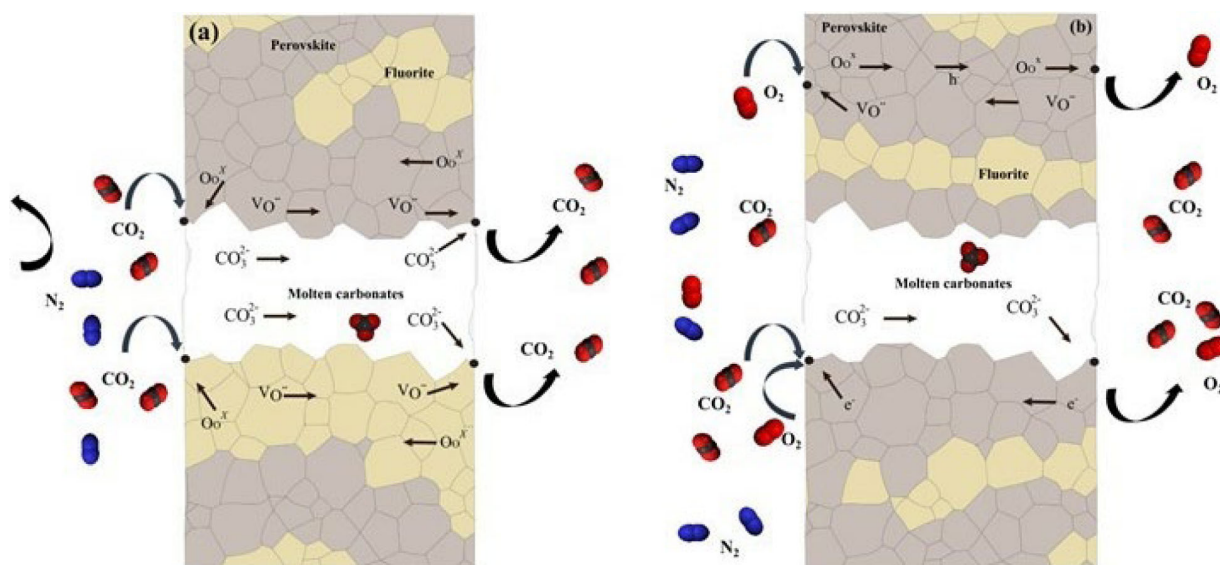
conduction properties of ceramic phase.

Additionally, considering a chemical gradient of $O_2$, reaction (Eq. (3)) must be also considered. In this latter case the transport of oxygen takes place through the ceramic phase, following an oxygen vacancy mediated transport mechanism.

$$\frac{1}{2}O_2 + V_{\ddot{O}} \leftrightarrow O_O^x + 2\dot{h} \qquad (3)$$
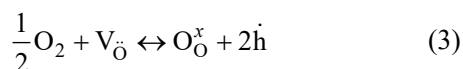
Recently, a novel sort of MIECC-based ceramic–carbonate membrane has been reported [23–25]. The distinctive feature of this membrane is that ceramic phase is made of a fluorite–perovskite composite exhibiting well separated grains of the two phases; which are an oxygen ionic conductor ($Ce_{0.85}Sm_{0.15}O_2$) and an ionic–electronic conductor ($Sm_{0.6}Sr_{0.4}Al_{0.3}Fe_{0.7}O_3$)

respectively. This ceramic–carbonate membrane shows excellent perm-selectivity properties and simultaneous high $CO_2/O_2$ permeation flux density at elevated temperatures between 700 and 900 ℃ [23]. Considering the properties of the composite ceramic phase, the transport of $CO_2$ and $O_2$ species must involve the three previously discussed mechanisms (Eqs. (1)–(3)), as depicted in Fig. 1.

Currently, there is plenty of information about the design of oxygen-selective membranes that present mixed ionic–electronic conduction [26–32]; the studied systems include dense membranes made of fluorite–perovskite composite ceramics (Table 1). This kind of membranes shows high oxygen permeation flux at high temperature as well as great chemical stability under atmospheres containing $CO_2$. This suggests that, like in previous



**Fig. 1** Transport mechanism for simultaneous $CO_2$ and $O_2$ species that involves three different pathways: (a) perm-selective transport of $CO_2$ based on the oxygen ionic conduction properties of ceramic phases, and (b) perm-selective transport of oxygen and simultaneous transport of $CO_2/O_2$ due to the mixed electronic–ionic conduction properties of the perovskite phase.

**Table 1　Composition and oxygen permeation features of dense membranes made of fluorite and perovskite ceramics**

| Membrane composition | | Thickness (mm) | Observed oxygen permeation flux* (mL·cm$^{-2}$·min$^{-1}$) | Reference |
| --- | --- | --- | --- | --- |
| Fluorite | Perovskite | | | |
| $Ce_{0.8}Sm_{0.2}O_{2-\delta}$ (75 wt%) | $Sm_{0.8}Ca_{0.2}Mn_{0.5}Co_{0.5}O_{3-\delta}$ (25 wt%) | 0.5 | 0.39 | [26] |
| $Ce_{0.8}Gd_{0.15}Cu_{0.05}O_{2-\delta}$ (80 wt%) | $SrFeO_{3-\delta}$ (20 wt%) | 0.5 | 0.56 | [27] |
| $Ce_{0.9}Pr_{0.1}O_{2-\delta}$ (60 wt%) | $Pr_{0.6}Sr_{0.4}FeO_{3-\delta}$ (40 wt%) | 0.6 | 0.16 | [28] |
| $Ce_{0.8}Sm_{0.2}O_{1.9}$ (75 wt%) | $Sm_{0.8}Ca_{0.2}Mn_{0.5}Co_{0.5}O_3$ (25 wt%) | 0.5 | 0.4 | [29] |
| $La_{0.15}Ce_{0.85}O_{2-\delta}$ (70 wt%) | $La_{0.15}Sr_{0.85}FeO_3$ (30 wt%) | 0.6 | 0.32 | [30] |
| $La_{0.15}Ce_{0.8}Cu_{0.05}O_{2-\delta}$ (70 wt%) | $La_{0.15}Sr_{0.85}FeO_3$ (30 wt%) | 0.6 | 0.45 | [30] |
| $Ce_{0.85}Gd_{0.1}Cu_{0.05}O_{2-\delta}$ (75 wt%) | $La_{0.6}Ca_{0.4}FeO_{3-\delta}$ (25 wt%) | 0.5 | 0.61 | [31] |
| $Ce_{0.9}Pr_{0.1}O_{2-\delta}$ (60 wt%) | $Pr_{0.6}Sr_{0.4}Fe_{0.5}Co_{0.5}O_{3-\delta}$ (40 wt%) | 0.6 | 0.59 | [32] |

*The values of permeation flux correspond to an operating temperature of 900 ℃.

reports [23,24], if a molten carbonate phase is incorporated, these composite systems could be used in MIECC-based membranes for the concomitant $CO_2$ and $O_2$ separation.

This work aims to inquire on the feasibility to process ceramic–carbonate membranes, where the ceramic phase is composed in turn, of a mixture of fluorite and perovskite phases. The selected systems are the $Ce_{0.85}Gd_{0.1}Cu_{0.05}O_{2-\delta}$–$La_{0.6}Ca_{0.4}FeO_3$ and $Ce_{0.9}Pr_{0.1}O_{2-\delta}$–$Pr_{0.6}Sr_{0.4}Fe_{0.5}Co_{0.5}O_{3-\delta}$ composites (Table 1). If a membrane can be processed showing thermal and chemical stability, as well as high selectivity of $CO_2$ and $O_2$ then, such membrane can be used in the design of membrane reactors, for example in the dry-oxy methane reforming reaction for syngas production.

## 2　Experimental procedure

### 2.1　Synthesis of the fluorite–perovskite composite powders

Two different fluorite/perovskite composite powders were prepared, specifically, the $Ce_{0.85}Gd_{0.1}Cu_{0.05}O_{2-\delta}$–$La_{0.6}Ca_{0.4}FeO_3$ (75 wt%–25 wt%) and $Ce_{0.9}Pr_{0.1}O_{2-\delta}$–$Pr_{0.6}Sr_{0.4}Fe_{0.5}Co_{0.5}O_{3-\delta}$ (50 wt%–50 wt%) compositions which were labeled as 75CGCO–25LCF and 50CP–50PSFC respectively. The powders were chemically synthesized by the so-called one-pot method which is based on the combined ethylene-diamine-tetra acetic acid (EDTA)/citrate complexing method to produce crystalline complex oxides as a final product [23–25]. Briefly, aqueous metal nitrates solutions with the corresponding stoichiometric amounts of precursors were prepared starting from $Ce(NO_3)_3 \cdot 6H_2O$ (99.0% Sigma-Aldrich), $Gd(NO_3)_3 \cdot 6H_2O$ (99.9% Alfa Aesar), $Cu(NO_3)_2 \cdot 3H_2O$ (99% Meyer), $La(NO_3)_3 \cdot 6H_2O$ (99% Acros Organics), $Ca(NO_3)_2 \cdot 4H_2O$ (99% Meyer), and $Fe(NO_3)_3 \cdot 9H_2O$ (99% Meyer) nitrates to prepare the 75CGCO–25LCF phase; additionally, $Pr(NO_3)_3 \cdot 6H_2O$ (99.9% Sigma-Aldrich), $Sr(NO_3)_2$ (99% Meyer), and $Co(NO_3)_2 \cdot 6H_2O$ (99% Meyer) were used for the 50CP–50PSFC phase. A molar ratio of EDTA:citric:total metal cations was established as 1:1:1.5. The pH values for the solution precursors were adjusted to 9 by adding ammonium hydroxide (28.0%–30.0% J.T. Baker). These solutions were subsequently heated up to 90 ℃ under constant stirring until a viscous gel was obtained in both cases. Then each gel was heated up to 300 ℃ to promote its self-combustion, removing the organic matter

and obtaining of the powders. Further calcination of the powders was carried out at 600 ℃ for 10 h under air atmosphere to obtain the crystalline 75CGCO–25LCF and 50CP–50PSFC phases.

### 2.2　Preparation of ceramic–carbonate dual-phase membranes

Firstly, disk-shaped porous membrane supports were fabricated by uniaxial pressing and incipient sintering. The 75CGCO–25LCF disks were sintered at 900 ℃ for 10 h, while 50CP–50PSFC disks were heat treated at 1050 ℃ for 10 h. These sintering conditions were set based on the dilatometric measurements. For both cases a ramping rate of heating and cooling was 2 ℃·min$^{-1}$ using an air atmosphere. Additionally, some dense disks were also prepared to perform a molten carbonates wettability test. Subsequently, dense dual-phase membranes (ceramic–carbonate) were prepared by direct infiltration of an eutectic molten carbonate ternary mixture ($Na_2CO_3$ (98% Alfa Aesar), $Li_2CO_3$ (99% Alfa Aesar), and $K_2CO_3$ (99% Alfa Aesar) in a 42.5/32.5/25 molar ratio), into the pores of the sintered 75CGCO–25LCF and 50CP–50PSFC supports, following the methods previously reported [16,17]. After the membrane infiltration and cooled down stages, the residual carbonate on the membrane surface was removed using SiC polishing paper. Thermal and chemical stability experiments were carried out for the different supports in different atmospheres at temperatures between 700 and 1200 ℃; the experiments consisted in placing the samples inside to a tubular furnace under a constant air or $CO_2$ flow rate of 60 mL·min$^{-1}$ for 20 h, and this showed the structural and chemical stability of the supports and membranes exposed to a rich oxygen or $CO_2$ environment.

### 2.3　Powder, support, and membrane characterization

The crystalline phases in 75CGCO–25LCF and 50CP–50PSFC samples were characterized by X-ray diffraction (XRD) technique, using a Bruker diffractometer model D8 Focus, equipped with a Cu Kα radiation source. Samples were measured in 2-theta range from 20° to 80° and the different phases were identified using the Powder Diffraction File (PDF-2) database. Non-isothermal dilatometric measurements were carried out on green supports using a Setaram SET-Sys-Evolution TMA equipment to examine the

sintering behavior of composite supports in a range of temperatures of 40–1300 ℃ under air atmosphere. A JEOL, JSM-6400 scanning electron microscope was used to characterize the microstructural features of both supports and dense dual-phase membranes. The supports porosity volume was determined by the Archimedes method based on the international standards ASTM C373-88. Unsteady state He permeation tests were used to elucidate the obtaining of an interconnected porosity in the supports as well as to demonstrate the high density of the infiltrated dual-phase membranes. Additionally, the wettability properties of fluorite–perovskite materials with the studied ternary molten carbonate mixture were evaluated by measuring the contact angle following the sessile drop method [26]. Briefly, a carbonate pellet is sited on the prepared highly dense disk ceramics samples, and it is heating up to 525 ℃ in vacuum. At this temperature carbonate pellet is completely melted and forms a drop. Once the liquid carbonate spreads on to the top surface of the dense disks, the contact angle is quantified by the so-called low bond axisymmetric drop shape analysis method (LB-ADSA), by using the ImageJ software [27].

## 2. 4 High temperature $CO_2/O_2$ permeation measurements and stability test

Permeation measurements were performed using a Probostat high temperature permeation system (NORECS AS), wherein ceramic–carbonate membranes were sealed to an inner alumina tube by using a silver sealant. The system was completely sealed into an outer highly dense alumina tube and heated at a rate of 3 ℃·min$^{-1}$ from room temperature to the desired temperature set point. Figure 2 shows a simple outline of the experimental
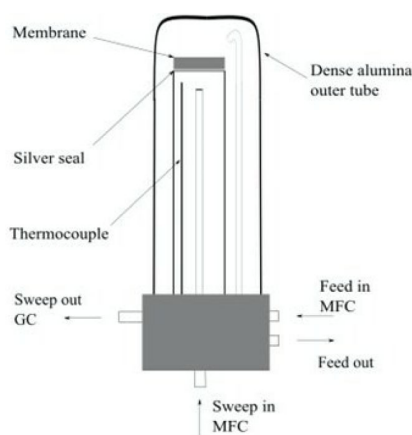


**Fig. 2** Schematic representation of the high temperature permeation setup for testing ceramic–carbonate membranes.

permeation setup which is equipped with a FCMix mass flow controller (NORECS AS). First, the $CO_2/O_2$ permeation properties of the 75CGCO–25LCF and 50CP–50PSFC-based ceramic–carbonate membranes were tested as a function of temperature from 850 to 940 ℃. Then, membranes were exposed to constant experimental conditions of 875 ℃ for a long term of 100 h.

The feed gas mixture used for the permeation experiments was $CO_2/O_2$ (15/17 mL·min$^{-1}$) $N_2$ balanced to 100 mL·min$^{-1}$. In all the cases, Ar was used as sweep gas in the downstream side of the membrane. The permeated gas and the gas leak were analyzed using a GC-2014 chromatograph (SHIMADZU) equipped with TCD detector and a Carboxen-1010 PLOT capillary column (30 m long and 0.32 mm in diameter). The gas leak was determined by the concentration of nitrogen in the effluent sweep gas.

## 3 Results and discussions

### 3. 1 Thermochemical stability under air and $CO_2$ rich atmospheres

To test the thermochemical stability, powders were calcined at 600, 900, 1000, 1100, and 1200 ℃ for 10 h in air. Figures 3(a) and 3(b) show the diffraction patterns of the 50CP–50PSFC and 75CGCO–25LCF calcined powders respectively at different temperatures. It was observed that samples without calcining have low crystallinity. At temperatures higher than 600 ℃, better crystallinity was observed, although it seems to be that the fluorite phase requires higher temperatures as compared to perovskite phase. At temperatures higher than 900 ℃, both the fluorite and perovskite phases showed sharp diffraction peaks. The CGCO and CP fluorite-type phases in the samples were identified using the JCPDS database card number 00-043-1002; then the obtained X-ray diffraction patterns are compatible with the *Fm-3m* (225) space group with a *fcc* crystal system. On the other hand, the perovskite LCF and PSFC phases were identified with the JCPDS file numbers 00-040-0224 and 00-028-1227 respectively; in both cases these cards correspond to cubic perovskite-type oxides. The thermal stability analysis shows no evidence of decomposition, even at 1200 ℃. These results suggest that both fluorite–perovskite composite systems are thermally stable throughout the operative temperature range. Moreover, it is important
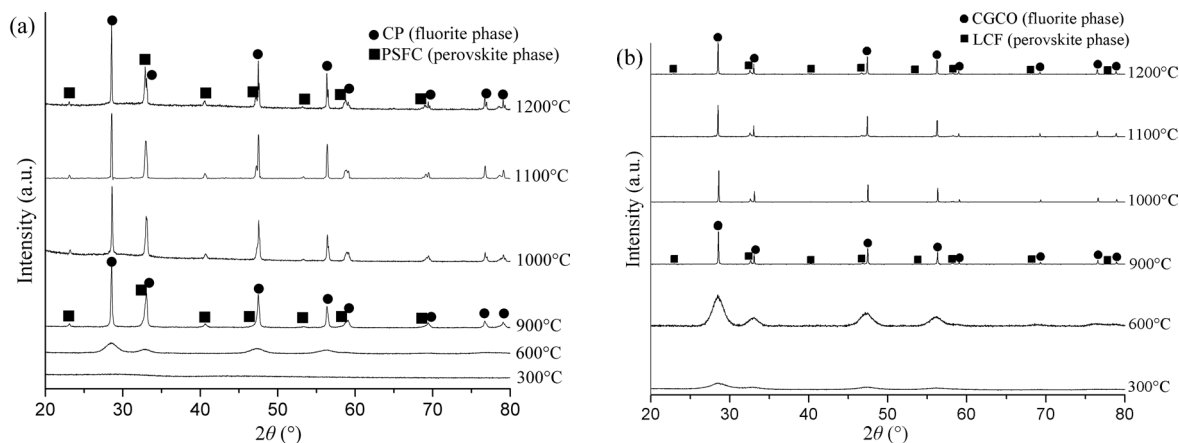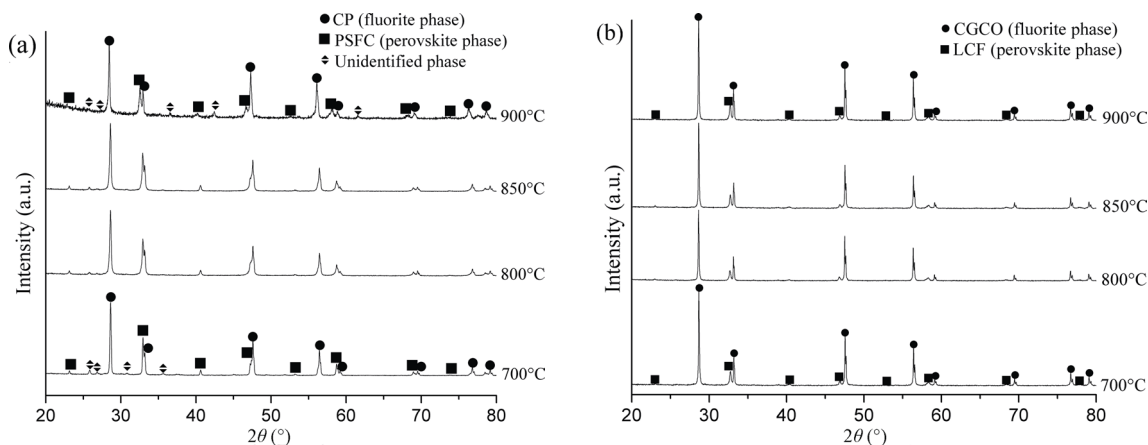
**Fig. 3** XRD patterns of (a) 50CP–50PSFC and (b) 75CGCO–25LCF calcined powders respectively at different temperatures.

to mention that this temperature range matches with the operative temperatures for certain reactors that utilize ceramic membranes; for example, to produce syngas through the so-called dry reforming and the oxy-dry reforming of methane the operative temperatures are typically between 700 and 875 ℃ [13,35,36].

As mentioned, one of the most attractive properties of fluorite–perovskite composites for the manufacture of membranes is their chemical stability under $CO_2$ containing atmospheres [23–25,37]. This property is a fundamental requirement for its application in membranes for $CO_2$ separation [16,18,23] and membrane reactors [38]. The chemical tolerance to $CO_2$ of the different membrane supports was determined experimentally by its exposure to a 100% $CO_2$ atmosphere. Figure 4 shows the XRD patterns for the porous support samples that were subjected to the chemical stability test in a $CO_2$ atmosphere between 700 and 900 ℃ during 20 h. It was observed that in the case of 75CGCO–25LCF sample (Fig. 4(b)), fluorite and perovskite phases are

present, with no formation of secondary oxide phases or metal carbonates in the range of temperatures studied. On the other hand, for 50CP–50PSFC porous support, XRD patterns (Fig. 4(a)) show the formation of small quantities of a secondary phase that could be attributed to the incipient surface reactivity of the materials with $CO_2$. The carbonates of alkaline elements are commonly the reaction products; however, in this work it was not possible to identify the new formed phases with the databases consulted. Same as before, $Ce_{0.9}Pr_{0.1}O_{2-\delta}$ (CP) and $Pr_{0.6}Sr_{0.4}Fe_{0.5}Co_{0.5}O_{3-\delta}$ (PSFC) phases were identified by card numbers 00-43-1002 and 00-28-1227, respectively, with no significant changes observed in the XRD reflections of these phases. In order to avoid these unknown phases, the system 50CP–50PSFC fluorite–perovskite could be operated at lower temperatures than the 75CGCO–25LCF system. In fact, results further reported in Section 3.4 revealed that 50CP–50PSFC based ceramic–carbonate membranes are stable at 875 ℃ under a $CO_2$ atmosphere.



**Fig. 4** XRD patterns of (a) 50CP–50PSFC and (b) 75CGCO–25LCF supports after exposure to a rich $CO_2$ atmosphere at different temperatures during 20 h.
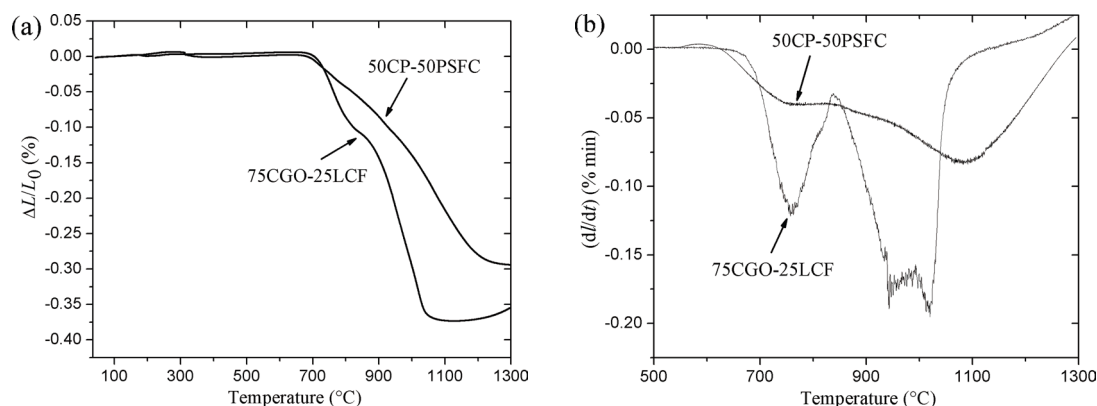
## 3. 2 Porous support and dense membrane fabrication

One way to produce porous supports is by controlling the densification process. Sintering is a densification process where the total porosity volume always decreases with increasing the temperature. Controlling the sintering process, it is possible to obtain an adequate microstructure of the membrane support [17]. Therefore, the green fluorite–perovskite supports were characterized by dilatometry studies to establish the sintering conditions to produce the supports. The dynamic sintering curves were obtained (Fig. 5(a)). Shrinkage starts around 670 ℃ in both systems but ends at different temperatures in each system. Sample 50CP–50PSFC does not shrink any more at 1300 ℃ while in the system 75CGCO–25LCF this fact occurs at 1100 ℃. Moreover, it was observed that densification process presents at least two stages (Fig. 5(b)), which is indicative of the obtaining of a heterogeneous packing of powders in the green compacts due to the presence of aggregates [39,40]. No further effort was done to elucidate with precision the presence of multi-step during sintering processes. In short, in order to have porous supports, subsequent green disks of 75CGCO–25LCF and 50CP–50PSFC systems were sintered at 900 and 1050 ℃ respectively for 10 h. On one hand, by reaching these temperatures it ensures that the phases of interest are well crystallized (Figs. 3(a) and 3(b)). Moreover, these temperatures were determined following the rational that at these temperatures the first stage of sintering has already occurred, but the shrinkage has not finished, that is, densification stage is still in progress, and hence some interconnected porosity remains.

Some microstructural characteristics of supports are shown in Table 2. It is shown the obtained open porosity, tortuosity, and unsteady state He permeance values, the latter in the order of $10^{-6}\,\text{mol·m}^{-2}\text{·s}^{-1}\text{·Pa}^{-1}$.

Dense samples of both systems were fabricated by sintering at 1200 ℃ for 15 h. These samples were meant to carry out wetting measurements and determine whether molten carbonates can properly wet the ceramic phases or not. Figure 6 shows a sequence of images recorded during the wetting experiments on the 50CP–50PSFC dense disk. Taking into account that the reported melting point of the mixture of carbonates is 397 ℃ [7], the pellet of carbonates at 325 ℃ is still in solid state but at 425 ℃, a significant amount of liquid phase is already observed. When the temperature reaches 525 ℃, the carbonates have melted completely. The contact angle of molten carbonates on 75CGCO–25LCF and 50CP–50PSFC substrates show values of 12.2° and 13.5° respectively; this low value reveals the

**Fig. 5** Dilatometric curves of 75CGCO–25LCF and 50CP–50PSFC samples under air atmosphere up to 1300 ℃: (a) linear shrinkage and (b) shrinkage rate.

**Table 2 Microstructural and permeation features of porous supports and dense membranes**

| Membrane support (fluorite–perovskite) | Ceramic phase (apparent vol%) | Carbonate phase[*] (vol%) | Support tortuosity[**] | He permeance (mol·m⁻²·s⁻¹·Pa⁻¹) | |
|---|---|---|---|---|---|
| | | | | Membrane support | Dense membrane[***] |
| 75CGCO–25LCF | 57 | 43 | 2.26 | $4.2\times10^{-6}$ | $3.05\times10^{-9}$ |
| 50CP–50PSFC | 71 | 29 | 1.02 | $7.9\times10^{-6}$ | $0.14\times10^{-10}$ |

[*]Carbonate phase considering the complete infiltration of the total open porosity.
[**]Based on room temperature steady state helium permeance measurements before molten carbonate infiltration.
[***]Room temperature unsteady state helium permeance measurements after molten carbonate infiltration.

**Fig. 6** Wettability measurements wherein contact angle was analyzed using ImageJ software: (a) carbonate pellet on the 50CP–50PSFC substrate, (b) incipient melting of carbonate pellet, and (c) spread carbonate drop.

excellent wettability of the molten carbonates with respect to fluorite–perovskite phases. Complete wetting is desirable in the infiltration process; otherwise, a lack of wettability could result on the incomplete filling of porosity by carbonates and consequent poor values of selectivity during the permeation tests [15,20] and even more, the gradual loss of molten carbonates during the long-term operation [10]. Table 2 shows the helium permeance values obtained for the porous supports and the dense membranes. It is clear that the permeation flux decreases around 3–4 orders of magnitude after infiltration. This suggests that after infiltration, the pieces are very dense as a result of an efficient infiltration. The remaining low helium permeation exhibited by the membranes is caused by Knudsen flow, which occurs due to small gaps produced by the shrinkage of carbonate phases during cooling. Nevertheless, when the membranes are heated up to high operational temperature, molten carbonates melt again and experience a volume expansion occupying the remaining spaces in the pores. This phenomenon was corroborated during $CO_2/O_2$ permeation measurements presented below.
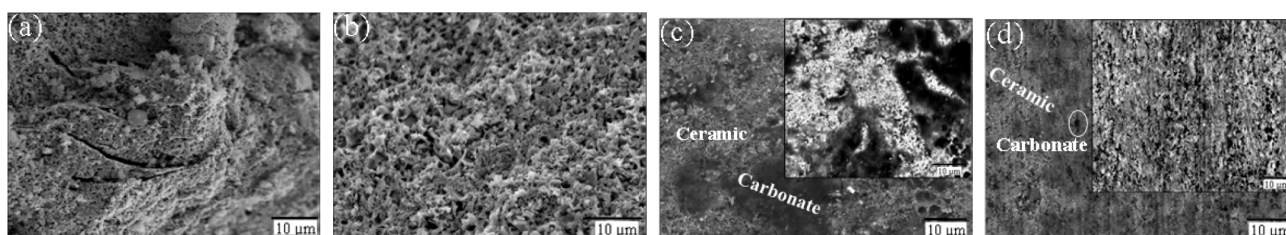
Figure 7 shows SEM images of the cross section of membrane supports (Figs. 7(a) and 7(b)) and the dense ceramic–carbonate membranes (Figs. 7(c) and 7(d)). Membrane supports are highly porous, which agrees with the pore volume fraction estimated by the Archimedes method (Table 2). Moreover, a more detailed analysis of the SEM images of samples suggests that pore size distribution is wide but in the micrometric range. 75CGCO–25LCF support exhibits pores between

0.5 and 2.0 μm. Smaller pores in the range of 0.25–1.5 μm were observed for the sample 50CP–50PSFC. Such small pores are convenient for infiltration purposes since the capillary pressure is inversely proportional to the pore size. A rough estimation of pressure difference values can be calculated by the Laplace equation assuming a straight pore (Eq. (4)).

$$r = \frac{2\sigma\cos\theta}{P' - P''} \tag{4}$$

In Eq. (4), $r$ is the pore radius of the support, $\sigma$ is the surface tension, and $\theta$ is the contact angle of the molten carbonates. Considering the biggest pore diameter observed by SEM of about 2.0 and 1.5 μm for the supports 75CGCO–25LCF and 50CP–50PSFC respectively, and following the procedure previously reported in Ref. [7], it can be argued that the fabricated ceramic–carbonate membranes can operate under a transmembrane pressure difference of 4.4 and 5.8 atm respectively without loss of the molten phase. Of course, these values are good and can be further improved by a better control of the microstructure of the support.

After infiltration, SEM analyses show the microstructure of the biphasic dense membranes that does not show the presence of big cracks (Figs. 7(c) and 7(d)). The interconnected porosity of the supports previously observed, was occupied by the molten carbonates. In Figs. 7(c) and 7(d), the infiltrated carbonates are clearly distinguished dark zones, contrasting to the bright white zones which correspond to the fluorite and perovskite phases.



**Fig. 7** SEM images of the cross section of (a) 50CP–50PSFC ceramic support, (b) 75CGCO–25LCF ceramic support, (c) 50CP–50PSFC/carbonates, and (d) 75CGCO–25LCF/carbonates dense dual phase membranes.

## 3. 3 High temperature CO₂–O₂ permeation measurements

The permeation properties of the ceramic–carbonate membranes were evaluated at temperatures between 850 and 940 ℃. As expected, membranes show a simultaneous permeation of $O_2$ and $CO_2$ (Figs. 8 and 9) with the typical behavior already reported, regarding the increase of the permeation flux values ($J_{O2}$ and $J_{CO2}$) as a function of the temperature [16,20,23,41]. This fact confirms that the diffusion of the species is thermally activated. It is remarkable the observed $CO_2$ permeance which reaches values around $4.5 \times 10^{-7}$ $mol \cdot m^{-2} \cdot s^{-1} \cdot Pa^{-1}$ in the case of 50CP–50PSFC based membrane (Fig. 8(a)) and around $2.5 \times 10^{-7}$ $mol \cdot m^{-2} \cdot s^{-1} \cdot Pa^{-1}$ for the membrane 75CGCO–25LCF at 940 ℃ (Fig. 9(a)); moreover, at the same temperature, $O_2$ permeance reaches significant values of $2.2 \times 10^{-7}$ and $0.68 \times 10^{-7}$ $mol \cdot m^{-2} \cdot s^{-1} \cdot Pa^{-1}$ respectively (Figs. 8(b) and 9(b)).

Different to the behavior of metal–ceramic membranes wherein the oxygen permeation flux is approximately the half of the carbon dioxide flux (according Eq. (1)); here, the composition of the permeated gas does not match to a $CO_2 : O_2$ molar ratio of 2 : 1. The possible reason is related to the different transport mechanisms involved (Eqs. (1)–(3)). Nevertheless, it is important to mention that by controlling the fluorite–perovskite composition (ratio), it can be controlled the permeated $CO_2 : O_2$ ratio, which opens the possibility of applying this kind of membranes for the design of certain reactors, for example the dry oxy-reforming of methane to produce syngas with a controllable $H_2/CO$ ratio.

Table 3 shows the values of the separation factor estimated in the whole range of temperature. In both systems, separation factors increase with the operating temperature. Considering a negligible contribution due to leaking (based on Knudsen flow of $N_2$) once the silver seal reaches gas-tight, then the trend can be
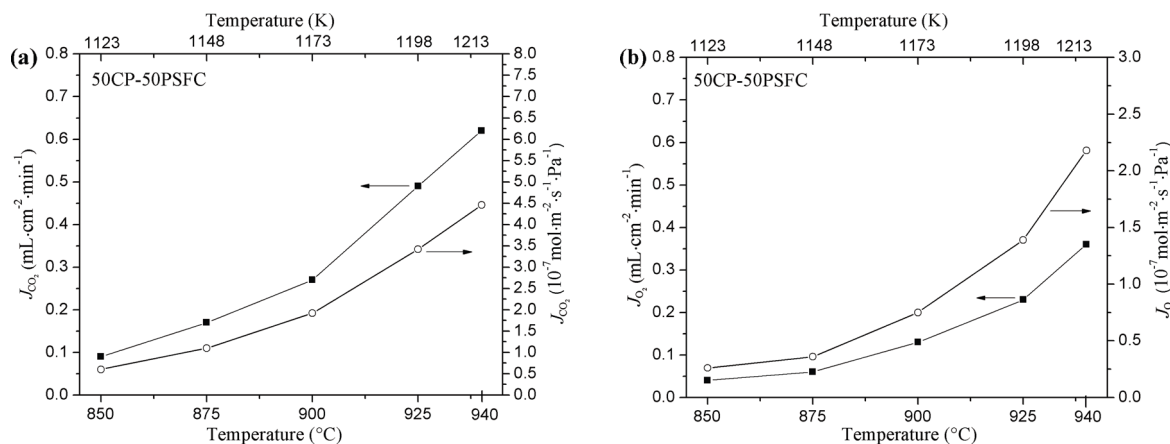


**Fig. 8** Experimental permeation fluxes observed in the studied temperature range for the 50CP–50PSFC/carbonate membrane: (a) $J_{CO_2}$ and (b) $J_{O_2}$.
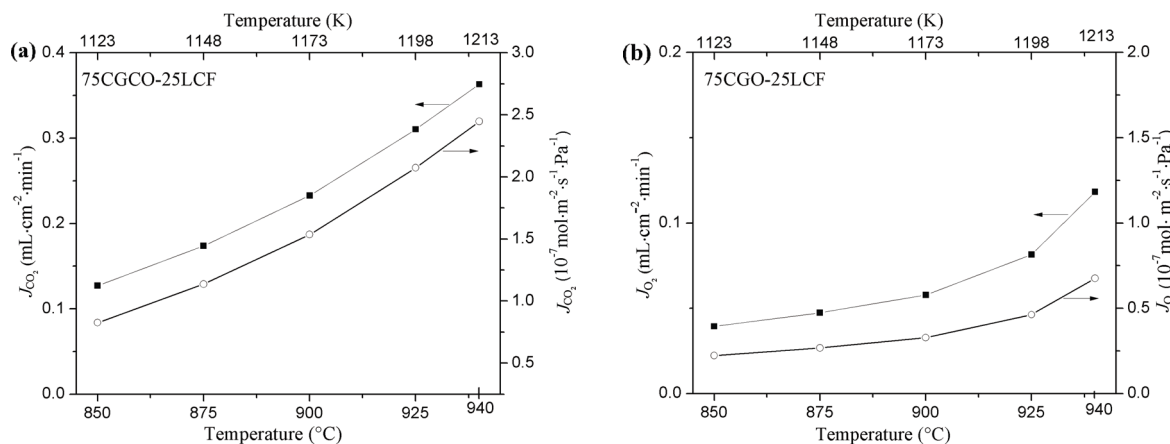


**Fig. 9** Experimental permeation fluxes observed in the studied temperature range for the 75CGCO–25LCF/carbonate membrane: (a) $J_{CO_2}$ and (b) $J_{O_2}$.

**Table 3  Separation factor and observed total permeance values ($J_{CO2}+J_{O2}$)**

| Membrane (fluorite–perovskite/carbonates) | Operating temperature (℃) | Separation factor | | Total permeance $J_{CO2}+J_{O2}$ $(10^{-7}\,mol\cdot m^{-2}\cdot s^{-1}\cdot Pa^{-1})$ |
|---|---|---|---|---|
| | | $CO_2/N_2$ | $O_2/N_2$ | |
| 75CGCO–25LCF/MC | 850 | 178 | 49 | 0.98 |
| | 875 | 244 | 59 | 1.41 |
| | 900 | 326 | 72 | 1.87 |
| | 925 | 435 | 101 | 2.53 |
| | 940 | 509 | 146 | 3.13 |
| 50CP–50PSFC/MC | 850 | 150 | 95 | 0.86 |
| | 875 | 276 | 117 | 1.46 |
| | 900 | 348 | 271 | 2.67 |
| | 925 | 781 | 335 | 4.81 |
| | 940 | 991 | 511 | 6.64 |

understood in terms of the temperature dependence of the permeation flux. Hence, the total permeation flux ($J_{CO_2}+J_{O_2}$), for the system 50CP–50PSFC, increases from $0.86\times10^{-7}$ to $6.64\times10^{-7}$ mol·m$^{-2}$·s$^{-1}$·Pa$^{-1}$ when the temperature changes from 850 to 940 ℃. This is in our understanding one of the highest permeation values obtained so far for this kind of ceramic–carbonate membranes under similar operation conditions. Once again, the observed combined flux of $CO_2$ and $O_2$ give guidelines to think on certain applications such as the experimentally demonstrated membrane reactor for oxy-dry reforming of methane with the $CO_2$ separated from flue gas [13]. More results on our efforts in this direction will be reported in the near future.

### 3.4  High temperature long-term stability test

Figure 10 shows the $CO_2$ and $O_2$ permeation stability tests for 100 h or a little more than 4 days. These long-term tests were carried out at 875 ℃. At the beginning of the tests, the two membranes experience certain unsteady period wherein $CO_2$ permeation flux rises abruptly with time (Fig. 10(a)); however, in both cases, after around 20 h operating, the membranes exhibit a stable permeation flux of $CO_2$ and $O_2$ for the rest of the 100 h. This feature has been largely reported and it can be the result of many factors, for example, certain microstructural changes in the membrane; however, this instability can be considered minor [42–45]. Additionally, in the case of ceramic–carbonate membranes, this behavior could also be related with the presence of small amounts of molten carbonates on the external surface of the membranes that hinders the surface reactions in the early stage of the tests. It is remarkable that no leaks were observed during the long periods of exposure nor reductions in permeation properties. These results are promising and bring to light the stability properties of the proposed fluorite–perovskite composites. In other fluorite- or perovskite-based single systems, the decomposition of the ceramic phase in ceramic–carbonate membranes has been reported but it remains as unsolved
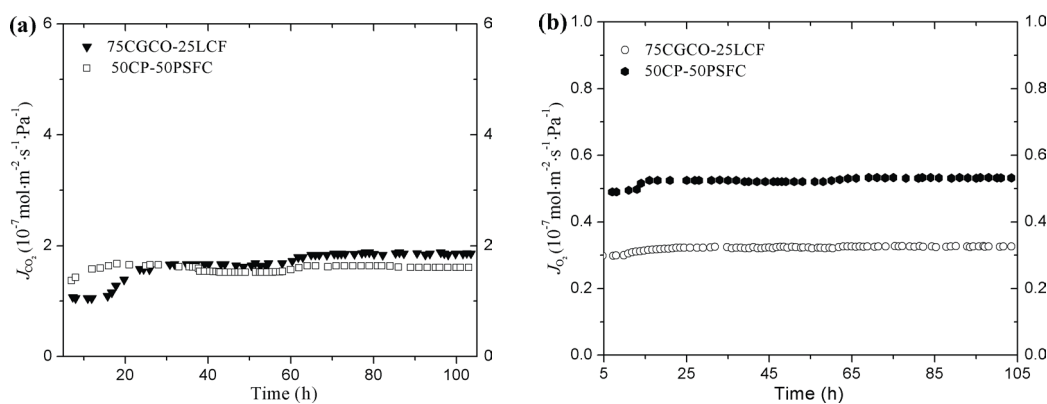


**Fig. 10**  Long-term permeation stability test performed at 875 ℃ using 85%air/15%$CO_2$ as feed gas and argon as sweep gas: (a) $J_{CO_2}$ and (b) $J_{O_2}$ for the 100 h test.

issue [18–46,47].

Figure 11 shows the SEM images of the feed and sweep side surface of the membranes after 100 h of exposure to experimental conditions at 875 ℃. As shown, both the feed and sweep sides of the membranes still exhibit the dual-phase microstructure. However, tested membranes show certain microstructural changes, such as increase in grain size, which can be noticed when compared to fresh membranes (Fig. 7). The feed side surface of the membranes clearly shows a dense dual-phase microstructure while the sweep side shows a small increase of the porosity in comparison with the fresh membranes. This behavior has been previously reported in other ceramic–carbonate systems [18] and it is assumed that different to the feed side, the experimental conditions in the sweep involves a much lower partial pressure of $CO_2$ that promotes the carbonate decomposition at the top surface. Nevertheless, as no $N_2$ leaks were observed during the long-term test, carbonate lost can be negligible. Therefore, generally speaking, the studied membrane systems can be considered highly stables.

Finally, the chemical stability of the studied fluorite–perovskite ceramic phases in the $CO_2$ can be analyzed from the thermodynamic point of view; Fig. 12 shows the Gibbs energy change for carbonate formation considering the single oxide constituents in the ceramic phases. Calculations were performed by using the FactSage thermochemical software [48]. In Fig. 12, the thermodynamic data for carbonate formation was obtained for a wide range of temperatures including the operating conditions of the membranes. The values of partial pressure used in calculations correspond to the $P_{CO2}$ for the feed and sweep atmosphere. Briefly, based on the criteria for equilibrium, Gibbs free energy values for the carbonation reactions show that only the $SrCO_3$ is able to be formed under the feed side conditions. Nevertheless, as the permeation properties showed no
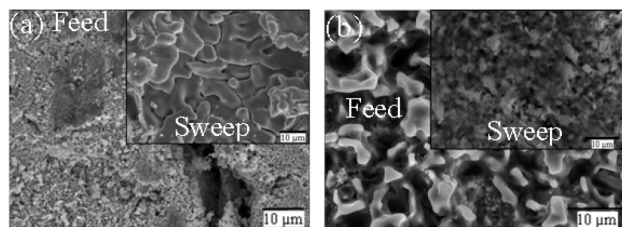


**Fig. 11** SEM analysis of the feed and sweep side of the membranes after 100 h exposure to $CO_2$ and $O_2$ with 85%air/15%$CO_2$ at 875 ℃: (a) 50CP–50PSFC and (b) 75CGCO–25LCF ceramic–carbonate membrane.
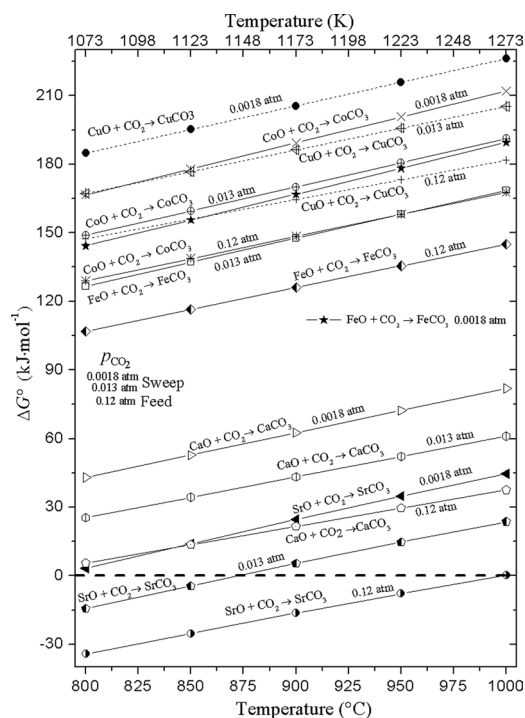


**Fig. 12** Gibbs energy change for carbonation reactions. The partial pressure in atm corresponds to the $P_{CO2}$ for the feed and sweep atmospheres.

significant diminishment during the long term stabillity test, it seems that the carbonation, if any, exhibites a low reaction rate, and it does not affect the membrane performance. In the same sense, although the thermodynamic data for lanthanide carbonates were not available, previous reports [49] suggest that $La_2(CO_3)_3$, $La_2O_2CO_3$, and $PrO_2CO_3$ species should not be stable under the operating membrane conditions, specially under those condition established for the long-term stabillity test.

Recapitulating, one of the main objectives of this research was the manufacture of dual phase ceramic–carbonate membranes using the systems 75CGCO–25LCF and 50CP–50PSFC as ceramics supports, to carry out the permeation and separation of $CO_2$ and $O_2$ by diffusion mechanisms at relatively high temperatures. Then, it is considered that this objective was satisfactorily accomplished.

## 4    Conclusions

Ceramic membranes were fabricated using two different formulations and their structure is based on the mixed ionic–electronic and carbonate-ion conductor (MIECC)

concept. The two fluorite–perovskite formulations, 75CGCO–25LCF–carbonate and 50CP–50PSCF–carbonate exhibited excellent simultaneous $CO_2/O_2$ permeation flux, reaching values of total permeation flux ($J_{CO_2}+J_{O_2}$) as high as $3.13\times10^{-7}$ mol·m$^{-2}$·s$^{-1}$·Pa$^{-1}$ and $6.64\times10^{-7}$ mol·m$^{-2}$·s$^{-1}$·Pa$^{-1}$ at 940 ℃ respectively. These values represent a significant improvement as compared to reported values for ceramic–carbonate membranes up to date. Moreover, the membranes reported in this work, show high selectivity and stability in long-term permeation operation. The high values of permeation flux reported here, suggest the possibility to apply these membranes in reactors for syngas production from dry reforming and dry-oxy reforming of methane processes. Further efforts will be done in this direction.

## Acknowledgements

## References

[1]  Koytsoumpa EI, Bergins C, Kakaras E. The $CO_2$ economy: Review of $CO_2$ capture and reuse technologies. *J Supercrit Fluids* 2018, **132**: 3–16.

[2]  Chung W, Roh K, Lee JH. Design and evaluation of $CO_2$ capture plants for the steelmaking industry by means of amine scrubbing and membrane separation. *Int J Greenh Gas Control* 2018, **74**: 259–270.

[3]  Espinal L, Poster DL, Wong-Ng W, *et al*. Measurement, standards, and data needs for $CO_2$ capture materials: A critical review. *Environ Sci Technol* 2013, **47**: 11960–11975.

[4]  Giordano L, Gubis J, Bierman G, *et al*. Conceptual design of membrane-based pre-combustion $CO_2$ capture process: Role of permeance and selectivity on performance and costs. *J Membr Sci* 2019, **575**: 229–241.

[5]  Giordano L, Roizard D, Favre E. Life cycle assessment of post-combustion $CO_2$ capture: A comparison between membrane separation and chemical absorption processes. *Int J Greenh Gas Control* 2018, **68**: 146–163.

[6]  Sherman SR, Gray JR, Brinkman KS, *et al*. Combustion-assisted $CO_2$ capture using MECC membranes. *J Membr Sci* 2012, **401–402**: 323–332.

[7]  Chung SJ, Park JH, Li D, *et al*. Dual-phase metal–carbonate membrane for high-temperature carbon dioxide separation. *Ind Eng Chem Res* 2005, **44**: 7999–8006.

[8]  Xu NS, Li X, Franks MA, *et al*. Silver-molten carbonate composite as a new high-flux membrane for electrochemical separation of $CO_2$ from flue gas. *J Membr Sci* 2012, **401–402**: 190–194.

[9]  Zhang LL, Gong YH, Brinkman KS, *et al*. Flux of silver-carbonate membranes for post-combustion $CO_2$ capture: The effects of membrane thickness, gas concentration and time. *J Membr Sci* 2014, **455**: 162–167.

[10] Zhang LL, Gong YH, Yaggie J, *et al*. Surface modified silver-carbonate mixed conducting membranes for high flux $CO_2$ separation with enhanced stability. *J Membr Sci* 2014, **453**: 36–41.

[11] Fang J, Tong JJ, Huang K. A superior mixed electron and carbonate-ion conducting metal-car bonate composite membrane for advanced flue-gas carbon capture. *J Membr Sci* 2016, **505**: 225–230.

[12] Fang J, Xu NS, Yang TR, *et al*. $CO_2$ capture performance of silver-carbonate membrane with electrochemically dealloyed porous silver matrix. *J Membr Sci* 2017, **523**: 439–445.

[13] Zhang P, Tong JJ, Huang K. Dry-oxy methane reforming with mixed e$^-$/CO$_3^{2-}$ conducting membranes. *ACS Sustainable Chem Eng* 2017, **5**: 5432–5439.

[14] Anantharaman R, Peters T, Xing W, *et al*. Dual phase high-temperature membranes for $CO_2$ separation – performance assessment in post- and pre-combustion processes. *Faraday Discuss* 2016, **192**: 251–269.

[15] Li YD, Rui ZB, Xia C, *et al*. Performance of ionic-conducting ceramic/carbonate composite material as solid oxide fuel cell electrolyte and $CO_2$ permeation membrane. *Catal Today* 2009, **148**: 303–309.

[16] Anderson M, Lin YS. Carbonate–ceramic dual-phase membrane for carbon dioxide separation. *J Membr Sci* 2010, **357**: 122–129.

[17] Ortiz-Landeros J, Norton T, Lin YS. Effects of support pore structure on carbon dioxide permeation of ceramic-carbonate dual-phase membranes. *Chem Eng Sci* 2013, **104**: 891–898.

[18] Norton TT, Ortiz-Landeros J, Lin YS. Stability of La–Sr–Co–Fe oxide–carbonate dual-phase membranes for carbon dioxide separation at high temperatures. *Ind Eng Chem Res* 2014, **53**: 2432–2440.

[19] Lan R, Abdallah SMM, Amar IA, *et al*. Preparation of dense La$_{0.5}$Sr$_{0.5}$Fe$_{0.8}$Cu$_{0.2}$O$_{3-\delta}$–(Li,Na)$_2$CO$_3$–LiAlO$_2$ composite membrane for $CO_2$ separation. *J Membr Sci* 2014, **468**: 380–388.

[20] Lu B, Lin YS. Synthesis and characterization of thin ceramic-carbonate dual-phase membranes for carbon dioxide separation. *J Membr Sci* 2013, **444**: 402–411.

[21] Zhang P, Tong JJ, Huang K. Self-formed, mixed-conducting, triple-phase membrane for efficient $CO_2/O_2$ capture from flue gas and *in situ* dry-oxy methane reforming. *ACS Sustainable Chem Eng* 2018, **6**: 14162–14169.

[22] Zhuang SJ, Han N, Xing M, *et al*. Perovskite oxide and carbonate composite membrane for carbon dioxide transport. *Mater Lett* 2019, **236**: 329–333.

[23] Ovalle-Encinia O, Pfeiffer H, Ortiz-Landeros J. $Ce_{0.85}Sm_{0.15}O_2$-$Sm_{0.6}Sr_{0.4}Al_{0.3}Fe_{0.7}O_3$ composite for the preparation of dense ceramic-carbonate membranes for $CO_2$ separation. *J Membr Sci* 2018, **547**: 11–18.

[24] Ovalle-Encinia O, Pfeiffer H, Ortiz-Landeros J. $CO_2$ separation improvement produced on a ceramic–carbonate dense membrane superficially modified with Au–Pd. *Ind Eng Chem Res* 2018, **57**: 9261–9268.

[25] Ovalle-Encinia O, Sánchez-Camacho P, González-Varela D, *et al*. Development of new bifunctional dense ceramic-carbonate membrane reactors for gas mixtures separation, through CO oxidation and subsequent $CO_2$ permeation. *ACS Appl Energy Mater* 2019, **2**: 1380–1387.

[26] Zhu XF, Liu HY, Cong Y, *et al*. Novel dual-phase membranes for $CO_2$ capture via an oxyfuel route. *Chem Commun* 2012, **48**: 251–253.

[27] Fang W, Steinbach F, Chen CS, *et al*. An approach to enhance the $CO_2$ tolerance of fluorite–perovskite dual-phase oxygen-transporting membrane. *Chem Mater* 2015, **27**: 7820–7826.

[28] Luo HX, Jiang HQ, Klande T, *et al*. Novel cobalt-free, noble metal-free oxygen-permeable $40Pr_{0.6}Sr_{0.4}FeO_{3-\delta}$–$60Ce_{0.9}Pr_{0.1}O_{2-\delta}$ dual-phase membrane. *Chem Mater* 2012, **24**: 2148–2154.

[29] Zhu XF, Liu HY, Cong Y, *et al*. Novel dual-phase membranes for $CO_2$ capture via an oxyfuel route. *Chem Commun* 2012, **48**: 251–253.

[30] Du ZH, Ma YH, Zhao HL, *et al*. High $CO_2$-tolerant and cobalt-free dual-phase membranes for pure oxygen separation. *J Membr Sci* 2019, **574**: 243–251.

[31] Fang W, Liang FY, Cao ZW, *et al*. A mixed ionic and electronic conducting dual-phase membrane with high oxygen permeability. *Angew Chem Int Ed* 2015, **54**: 4847–4850.

[32] Liang FY, Luo HX, Partovi K, *et al*. A novel $CO_2$-stable dual phase membrane with high oxygen permeability. *Chem Commun* 2014, **50**: 2451–2454.

[33] Gao LJ, Selman JR, Nash P. Wetting of porous $\alpha$-$LiAlO_2$ by molten carbonate. *J Electrochem Soc* 2018, **165**: F324–F333.

[34] Williams DL, Kuhn AT, Amann MA, *et al*. Computerized measurement of contact angles. *Galvanotechnik* 2010, **101**: 2502–2512.

[35] Wei YY, Yang WS, Caro J, *et al*. Dense ceramic oxygen permeable membranes and catalytic membrane reactors. *Chem Eng J* 2013, **220**: 185–203.

[36] Al-Fatesh A, Singh SK, Kanade GS, *et al*. Rh promoted and $ZrO_2$/$Al_2O_3$ supported Ni/Co based catalysts: High activity for $CO_2$ reforming, steam–$CO_2$ reforming and oxy–$CO_2$ reforming of $CH_4$. *Int J Hydrog Energy* 2018, **43**: 12069–12080.

[37] Zhang C, Sunarso J, Liu SM. Designing $CO_2$-resistant oxygen-selective mixed ionic–electronic conducting membranes: Guidelines, recent advances, and forward directions. *Chem Soc Rev* 2017, **46**: 2941–3005.

[38] Zhang P, Tong JJ, Huang K. Combining electrochemical $CO_2$ capture with catalytic dry methane reforming in a single reactor for low-cost syngas production. *ACS Sustainable Chem Eng* 2016, **4**: 7056–7065.

[39] Tian RF, Zhao F, Chen FL, *et al*. Sintering of samarium-doped ceria powders prepared by a glycine-nitrate process. *Solid State Ionics* 2011, **192**: 580–583.

[40] Shajahan I, Ahn J, Nair P, *et al*. Praseodymium doped ceria as electrolyte material for IT-SOFC applications. *Mater Chem Phys* 2018, **216**: 136–142.

[41] Yi JX, Zuo Y, Liu W, *et al*. Oxygen permeation through a $Ce_{0.8}Sm_{0.2}O_{2-\delta}$–$La_{0.8}Sr_{0.2}CrO_{3-\delta}$ dual-phase composite membrane. *J Membr Sci* 2006, **280**: 849–855.

[42] Zhu XF, Li QM, He YF, *et al*. Oxygen permeation and partial oxidation of methane in dual-phase membrane reactors. *J Membr Sci* 2010, **360**: 454–460.

[43] Zhu XF, Wang HH, Yang WS. Relationship between homogeneity and oxygen permeability of composite membranes. *J Membr Sci* 2008, **309**: 120–127.

[44] Kharton V, Naumovich E, Kovalevsky A, *et al*. Mixed electronic and ionic conductivity of $LaCo(M)O_3$ (M=Ga, Cr, Fe or Ni) IV. Effect of preparation method on oxygen transport in $LaCoO_{3-\delta}$. *Solid State Ionics* 2000, **138**: 135–148.

[45] Partovi K, Rüscher CH, Steinbach F, *et al*. Enhanced oxygen permeability of novel Cu-containing $CO_2$-tolerant dual-phase membranes. *J Membr Sci* 2016, **503**: 158–165.

[46] Gude U, Baumann S, Meulenberg WA, *et al*. Towards the development of materials for chemically stable carbonate-ceramic membranes to be used for $CO_2$ separation in water-gas-shift reactors. *Sep Purif Technol* 2019, **215**: 378–383.

[47] Chen TJ, Yu BL, Zhao YC, *et al*. Carbon dioxide permeation through ceramic-carbonate dual-phase membrane-effects of sulfur dioxide. *J Membr Sci* 2017, **540**: 477–484.

[48] Bale CW, Chartrand P, Degterov SA, *et al*. FactSage thermochemical software and databases. *Calphad* 2002, **26**: 189–228.

[49] Wei YY, Ravkina O, Klande T, *et al*. Effect of $CO_2$ and $SO_2$ on oxygen permeation and microstructure of $(Pr_{0.9}La_{0.1})_2(Ni_{0.74}Cu_{0.21}Ga_{0.05})O_{4+\delta}$ membranes. *J Membr Sci* 2013, **429**: 147–154.